Cinar, G., Mavris, D. N., Emeneth, M., Schneegans, A., Riediger, C., Fefermann, Y., & Isikveren, A. (2017). Sizing, integration and performance evaluation of hybrid electric propulsion subsystem architectures. In 55th AIAA Aerospace Sciences Meeting (p. 1183).

Sizing, Integration and Performance Evaluation of Hybrid Electric Propulsion Subsystem Architectures

Gokcin Cinar,* Dimitri N. Mavris,†
Aerospace Systems Design Laboratory, Atlanta, GA, 30332

Mathias Emeneth,‡ Alexander Schneegans§
PACE America Inc., Seattle, WA, 98115

Carsten Riediger,¶
328 Design GmbH, 82234 Wessling, Germany

Yann Fefermann,‖ Askin Isikveren,**
Safran Tech, Magny-Les-Hameaux, 78772, France

This paper presents a methodology for the sizing and synthesis of power generation and distribution (PG&D) subsystems. The PG&D subsystem models developed in a previous work done by the authors were applied within a parallel hybrid electric propulsion architecture using the Dornier 328 as the baseline aircraft. The hybridization took place only during the cruise segment. Analyses were performed in Pacelab SysArc, a system architecture design tool, to assess the impact of different hybrid electric propulsion architectures and changing PG&D subsystem characteristics at aircraft and mission levels. To this end, sensitivity analysis was conducted to reveal the sensitivity to the subsystem level characteristics. Moreover, six different architectures were compared in terms of their mission level performance. These architectures included the PG&D subsystems with current state of the art technology, NASA 15-year technology goals and a more advanced battery technology. Although neither the current state of the art PG&D subsystems nor NASA 15-year technology goals were advanced enough to match the design range requirement of the baseline aircraft, some of the competing architectures met the practical range target while enjoying substantial amount of fuel reductions. Finally, it was observed that in order to reach a break-even point in terms of the design mission range, a battery specific energy of 5 kWh/kg was necessary for a 50% level of hybridization during cruise. In this work the Dornier 328 was used as a testbed, however the methodology can be generalized for all parallel hybrid electric propulsion applications.

I. Introduction

A. The Need for a Greener Aviation

Over the last few years, there have been increasing efforts to reduce aviation related greenhouse gas emissions. In 2009, the ICAO Program of Action on International Aviation and Climate Change agreed to set a goal of 2% annual fuel efficiency improvement through the year 2050.[1] However, the European Commission on Climate Action reports that global aviation emissions by 2020 are forecasted to be 70% higher than in 2005 even with the annual 2% fuel efficiency improvement goal; noting that it could grow by a further 300-700% by 2050.[2]

*Graduate Researcher, School of Aerospace Engineering, Georgia Tech, AIAA Student Member
†S.P. Langley Distinguished Regents Professor and Director of ASDL, School of Aerospace Engineering, Georgia Tech, AIAA Fellow
‡Senior Business Development Manager, PACE America, AIAA Member
§President, PACE America, AIAA Member
¶Head of Flight Physics, 328 Design GmbH
‖System Architect, Energy and Propulsion Department, Safran Tech
**Head, Energy-Efficient Aircraft Architectures, Energy and Propulsion Department, Safran Tech, AIAA Member

ICAO has been working on developing a global certification standard for CO_2 emissions since 2010, aiming to promote more advanced fuel-efficient technologies (and hence enabling greater CO_2 reductions) than less advanced ones.[3,4] This standard would be applicable to both new aircraft designs as of 2020 and to new deliveries of current in-production aircraft types from year 2023.

As a response to the aforementioned demand for greener aviation, NASA N+3 goals (i.e. technologies nearing maturity in 2025) aim for more than 75% reduction in Landing Takeoff (LTO) NO_x emissions and more than 70% reduction in aircraft fuel burn with new cutting-edge aircraft designs and technology improvements.[5] These potential designs include but not limited to Bauhaus Luftfahrt's fully electric Ce-Liner concept, Boeing's SUGAR parallel hybrid electric aircraft concepts and NASA's N3X blended wing body concept.[5–8]

Although replacing conventional fuel burning engines with their electric counterparts would reduce CO_2 and NO_x emissions as well as noise, aircraft which solely depend upon electric motors and batteries are unlikely to achieve similar flight performance of conventional propulsion systems in the near future.[9,10] Hence, turbo-electric and hybrid-electric propulsion (HEP) systems are envisioned as a middle step towards all electric propulsion (EP) systems.

B. Sizing Challenges of Electric and Hybrid Electric Aircraft

Figure 1 shows a notional power train for EP, parallel and series HEP configurations where electrical energy is delivered from a battery to an electric motor. As it can be seen from Figure 1, the electrical energy is transmitted through common subsystem components in all three concepts; including but not limited to a battery as the primary or secondary energy source, a power converter for voltage and current conversions, an electric motor, generator, and transmission system. Throughout this paper, we will refer to these subsystem components as Power Generation and Distribution (PG&D) subsystems.

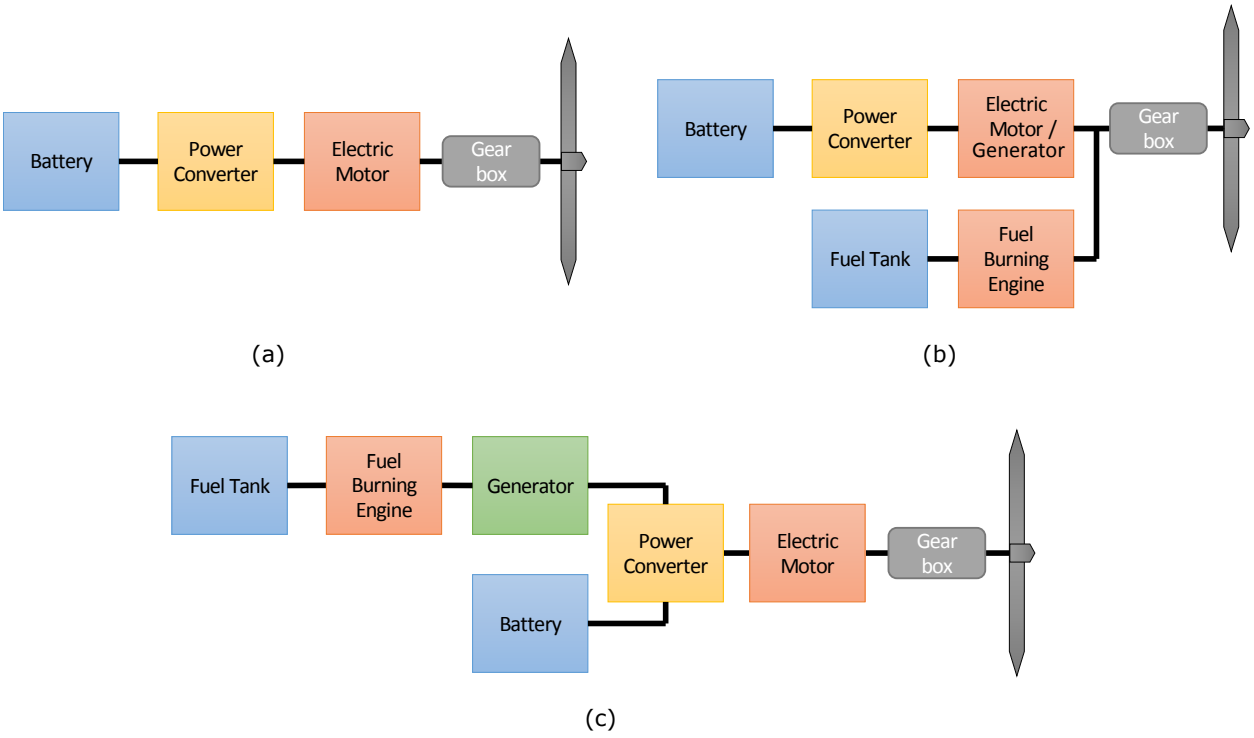

Figure 1. Notional subsystem components and powertrain for (a) Fully Electric propulsion, (b) Hybrid-electric propulsion connected in parallel, (c) Hybrid-electric propulsion connected in series

Traditionally, sizing of subsystem components is performed during conceptual aircraft design stage by using empirical relationships based concerning existing historical data.[11,12] From these empirical relations, information on aircraft weight, power (or thrust) and drag polar are then estimated and fed into the sizing and synthesis process where constraint analysis (to meet point performance requirements) and mission analysis (to fly a specific design mission) are carried out through iterations.[13] However, there is a lack of historical

data or readily available physics-based models for unconventional or more recent technologies such as ones that constitute PG&D subsystems. Moreover, the traditional sizing methods depend on the assumption that the time rate of change in aircraft weight equals the fuel flow, as used in the well-known Breguet range equation.[14] However this phenomena does not apply for EP technology as such systems might not lose weight over the course of a mission. Modifications to these methods are also necessary for hybrid-electric aircraft. Therefore, the empirical relations and methods given by the traditional design approaches cannot be directly used for such new concepts.

In previous work done by four of the authors, a methodology for evaluating subsystem level effects of EP technology on system level design metrics was proposed.[15] In another study, the authors developed detailed, physics-based, parametric subsystem models in order to perform comprehensive subsystem level analyses at the conceptual aircraft design stage.[16] These models not only provide more accurate results, but also are suitable for rapid and low cost analyses due to their parametric and easy-to-use nature. However, the need to project the effects of changing subsystem characteristics onto the overall vehicle design and mission performance still remains. Moreover, the magnitude of these effects will vary depending on which type of PG&D architecture is employed.

C. Objective and Proposed Approach

The main objective of this paper is to perform sensitivity analyses to reveal the possible impact of changing PG&D subsystem characteristics and to compare different hybrid-electric propulsion architectures at subsystem, system (vehicle) and mission levels. To this end, the following sections give a step by step explanation of the proposed approach which can be summarized as follows:

First, previously developed PG&D subsystem models by Cinar et al.[15] will be integrated within a parallel hybrid electric architecture. Second, a baseline aircraft which originally is powered by thermal engines will be retrofitted with this architecture. Third, the traditional aircraft sizing methodology will be modified to incorporate hybridization for a given design mission. Then, sensitivity analysis will be conducted to study sensitivity of important subsystem characteristics to some predetermined measures of performance (MoPs). Finally, six different architectures with different technology levels will be compared.

Before going into the details of the proposed approach, the system and mission level MoPs will be defined and a modeling environment will be chosen in the next paragraphs.

D. Measures of Performance

The flowchart in Figure 2 was proposed by Chakraborty and Mavris[17] for traditional aircraft and generalized here to include electric and hybrid electric aircraft. The flowchart demonstrates how a generic subsystem weight, drag, and power consumption or power losses due to inefficiencies cause an increment in the required power and hence the total required energy. For this study, PG&D subsystem components will be placed inside the vehicle except for the electric motor and therefore do not contribute to the zero-lift drag. It is also assumed that the zero-lift drag due to the exposed parts of the electric motor is negligible. It can be seen from the flowchart that additional subsystem weight not only increases the aircraft weight but also affects the overall required energy. This means that anything that changes the vehicle's weight and power consumption will change the overall vehicle design. It should also be noted that every component adds weight to the system, but may or may not directly draw power.

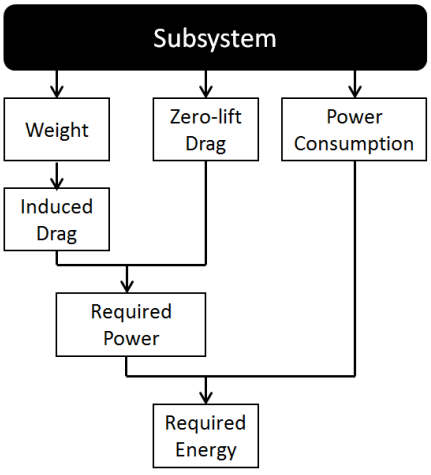

Figure 2. Effects of a generic subsystem on total energy required.

Because this is a retrofit study, the baseline aircraft will not be re-sized and therefore the maximum takeoff weight (MTOW) will be kept fixed and wings will not be resized. Along with MTOW, equipment weight fractions are also kept constant. However, introducing new subsystems will add extra weight to the system. Since the new components will be responsible for supplying a partial of the required power, the amount of required fuel will decrease. The changes in fuel and PG&D weight will result in changing equipment and structural weight,

and hence the operating empty weight (OEW; does not include PG&D weight). It would be the ideal case if the weight of the new subsystems could simply correspond to the extracted fuel weight for a given mission range. However, if the new subsystems weigh more than the maximum amount of fuel that can be replaced, then the aircraft will not be able to fly the same range anymore.

The other two factors that play an important role at the mission level are amount of fuel burn and state of charge of the battery. These factors can be combined within a single, unifying measure of total required energy.

To sum up, candidate architectures can be judged by the following MoPs: required energy, range and weight of the PG&D subsystem components. Additionally battery state of charge, fuel weight and OEW can also be tracked.

E. Modeling and Simulation Environment: Pacelab SysArc

The chosen modeling and simulation environment for system and subsystem level design and analysis is Pacelab SysArc which is a system architecture design tool. It allows to build, analyze and optimize system and subsystem architectures while instantly assessing their impact on the overall vehicles performance. It comes with an extensive library of different system components such as generators, motors, pumps, batteries, power converters etc., it creates automatically connecting distribution elements such as cables, pipes, ducts etc. and allows the application of different flight and failure modes on the architecture.

II. A Brief Overview of the PG&D Subsystem Models

This section gives a brief overview on the developed mathematical models of the subsystems that will be employed in PG&D architectures. These models consist of battery, power converter, electric motor, power distribution and management unit, and propeller speed reduction unit. The models were constructed as Engineering Objects (EO) within Pacelab SysArc Knowledge Designer, an environment where components can be characterized mathematically and defined geometrically. Once EOs are created, these building blocks become available to a component library which is used in the end-user application, Pacelab SysArc Engineering Workbench, to create the system models and analyze architectures. The interested reader is referred to Cinar et al.[15] for further details on the model development process.

A. Battery

Battery cells convert chemical energy to electrical energy through electrochemical reactions and generate DC electricity. This is called a "discharge" process. Rechargeable battery cells can reverse this chemical reaction when current is sent into the battery. This is called a "charge" process.[18]

The battery package is a very important component in electric and hybrid-electric vehicle applications as it is the main or secondary energy source and introduces a significant weight to the system.[15] Hence, choosing the right type and size of the battery is vital for the overall design.

There are various models on battery dynamics in literature, however it is important to find a suitable one that matches the level of complexity of the intended application while still yielding reliable results for conceptual design stage.

Equivalent circuit models can produce accurate results without going into details about battery chemistry provided that the model is properly built up to reflect battery characteristics. Hence, the battery model built into Pacelab SysArc was based on the rechargeable battery model presented by Tremblay and Dessaint.[19] Here, we shall give a brief summary of this model and quote a set of equations specifically for Li-Ion type of battery, but the interested reader can refer to Ref.[19] for further details and characteristics of other battery types.

Tremblay and Dessaint's model[19] takes two special points along with the extremes on a typical discharge characteristics curve given at a constant current to predict the battery behavior at any other current using a set of equations. In reference to Figure 3, the extremes are the fully charged voltage V_{full} (point a) and the maximum capacity Q (point d). The remaining two points are the so-called "end of the exponential zone" and "end of the nominal zone" which are given by points b (Q_{exp}, V_{exp}) and c (Q_{nom}, V_{nom}) in Figure 3, respectively. "End of the exponential zone" is the point at which the curve ends its exponential behavior at the beginning of discharge, whereas "the end of the nominal zone" is the point at which the voltage starts

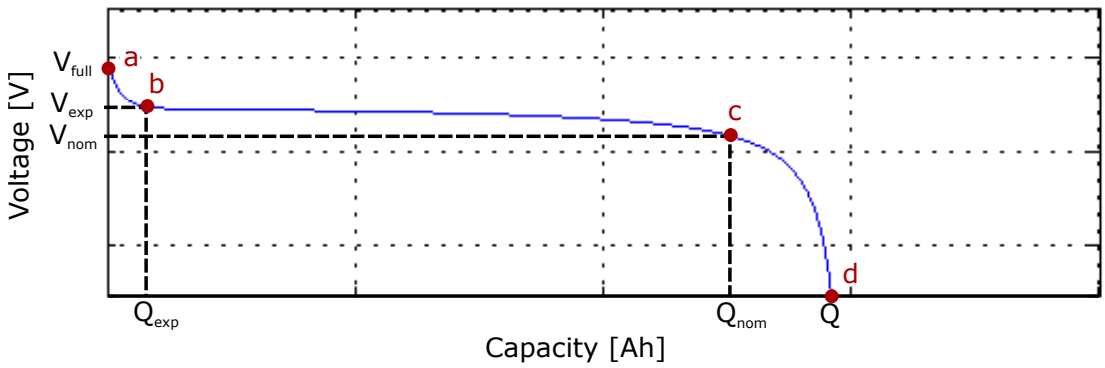

Figure 3. A sample discharge curve for a Lithium-Ion battery

to drop abruptly. The model also use an internal resistance (R). Then, the discharge and charge voltages are separately given as a function of capacity through a set of equations.

This model assumes that the internal resistance R remains constant and temperature effects and self-discharge of the battery are neglected. Furthermore, battery capacity is assumed to be independent of the current amplitude.

Table 1 provides a list of the input and output parameters of the battery model as implemented within Pacelab SysArc as an EO. The model uses cell characteristics (usually provided by the battery manufacturer) to build up the battery characteristics. The user also specifies the initial state of charge (SOC), discharge time and number of cells connected in parallel and series. Initial SOC and discharge time are used to calculate the final SOC. When the battery model is connected to a power load and the magnitude of the power requirement varies with time, discharge time becomes a set of time steps. For each time step, the model calculates the final SOC from initial conditions. Then, before going onto the next step, the initial conditions are overwritten by the final conditions of the previous step.

Especially if there are steep variations in amount of power required during time, then it is very important to keep these discharge times low in order to capture voltage and SOC variations. A battery can be damaged permanently if its SOC drops below a certain limit. For most battery types like lithium-ion batteries, this limit is taken as 20%.[18] Therefore, a minimum SOC limit can be set to prevent such permanent damage.

Finally, the model calculates the amount of energy required to supply the required power for a given amount of time. The user inputs battery energy-to-weight ratio (which is also called as "gravimetric specific energy") to calculate the weight of the battery.

As a result, the outputs are battery characteristics, final SOC, final battery voltage and weight. In Table 1, parameters with subscript "*cell*" stand for cell characteristics whereas those with subscript "*batt*" designate battery characteristics. The model also assumes that the battery efficiency is equal to the cell efficiency. Therefore, SOC and specific energy is equal at both the cell and battery levels.

The parameters shown on the input column must be given by the user so that the model can calculate the parameters shown in the output column. However, if two components are connected to each other, then some parameters (called "port parameter") are automatically propagated from one component to another. Such input port parameters which take their values from another component are designated with a "*" sign at the end of parameter descriptions in Table 1. Furthermore, Pacelab SysArc allows the user to toggle the input and output parameters provided that they are mathematically related. Therefore, if either of the input or output current value is known, then their input-output condition can be swapped.

It should also be noted that subsystem volume considerations are beyond the scope of this paper.

B. Power Converter

In the previous section, we explained how battery voltage changes as the battery is being discharged. However, the battery supplies energy to the electric motor or other non-propulsive subsystems which might work under different voltage demands. Hence, a nominal system voltage must be set independent of the battery voltage to provide consistency between other subsystem voltage requirements.

A power converter converts electrical power by changing input voltage to a desired voltage. However,

Table 1. Model input and output parameters of the Battery

Inputs			*Outputs*		
Parameter	Units	Description	Parameter	Units	Description
Nb_{ser}		Number of cells connected in series	Q_{batt}	[Ah]	Maximum capacity
Nb_{par}		Number of cells connected in parallel	$V_{full,batt}$	[V]	Fully charged voltage
Q_c	[Ah]	Maximum capacity	$I_{nom,batt}$	[A]	Nominal discharge current
$V_{full,cell}$	[V]	Fully charged voltage	R_{batt}	[Ω]	Internal resistance
$I_{nom,cell}$	[A]	Nominal discharge current	$V_{nom,batt}$	[V]	Nominal voltage
R, v	[Ω]	Internal Resistance	$Q_{nom,batt}$	[Ah]	Capacity at nominal voltage
$V_{nom,cell}$	[V]	Nominal voltage	$V_{exp,batt}$	[V]	Exponential zone voltage
$Q_{nom,cell}$	[Ah]	Capacity at nominal voltage	$Q_{exp,batt}$	[Ah]	Exponential zone capacity
$V_{exp,cell}$	[V]	Exponential zone voltage	$SOC_{f,batt}$	%	Final SOC
$Q_{exp,cell}$	[Ah]	Exponential zone capacity	$V_{batt,batt}$	[V]	Final voltage
$I_{disch,batt}$	[A]	Discharge current	W_{batt}	[kg]	Battery weight
SOC_i	%	Initial SOC			
SOC_{min}	%	Minimum SOC threshold			
Spec. Energy	[Wh/kg]	Energy to weight ratio (gravimetric specific energy)			

there will be a power loss due to inefficiencies of the converter and hence the useful output power will be less than the input power. The model developed for the power converter is depicted by Eqn. 1. The notations are explained in Table 2 and the port parameters are marked with a "*****" sign. The converter's weight is calculated from its power-to-weight ratio (i.e. gravimetric specific power) and nominal power.

$$\eta_{\mathbf{pc}}\mathbf{I_{in}}\mathbf{V_{in}} = \mathbf{I_{out}}\mathbf{V_{out}} \tag{1}$$

Table 2. Model input and output parameters of the Power Converter

Inputs			*Outputs*		
Parameter	Units	Description	Parameter	Units	Description
V_{out}	[V]	Voltage at the output terminal	I_{in}	[A]	Incoming Current
η_{pc}	%	Component efficiency	W_{pc}	[kg]	Component weight
P/W	[kW/kg]	Power to weight ratio			
P_{nom}	[kW]	Nominal power			
V_{out}	[V]	Voltage at the output terminal			
V_{in}	[V]	Voltage at the input terminal*			
I_{out}	[A]	Outgoing Current*			

C. Electric Motor

Electric motors convert electrical power to mechanical (shaft) power. They can operate at very high efficiency and have high reliability.[20] Electric motor efficiency is independent of operational altitude which gives an advantage over conventional internal combustion engines. The power losses in electric motors are mostly proportional to torque, which in turn is related to angular speed. The efficiency is also affected by the size of the motor and the cooling method.[18]

Performance of an electric motor is determined by its torque (T) and rotational speed (ω) characteristics. Shaft power (P_{mech}) is calculated using Eqn. 2, whereas electric power (P_{el}) is given by Eqn. 3.

$$\mathbf{P_{mech} = T\omega} \tag{2}$$

$$\mathbf{P_{el} = IV} \tag{3}$$

Generally, the torque of a DC motor is linearly proportional to the current traveling through its wires (also known as rotor or armature current). This relation is given by Eqn. 4 where k_T is the torque constant in [Nm/A] and I_A is the armature current in [A]. Value of the torque constant depends on the motor design. In case the torque-current relationship of a motor is more complex or completely unknown, the current going into the motor can still be found by Eqn. 4 to simplify the calculations.

$$\mathbf{T = k_T I_A} \tag{4}$$

Motors lose some of their input electrical power while converting to output mechanical power due to inefficiencies caused by various factors depending on the motor design, torque and speed. This conversion is given by Eqn.5 where η_{EM} is the electric motor efficiency.

$$\eta_{\mathbf{EM}} = \frac{\mathbf{P_{mech}}}{\mathbf{P_{el}}} = \frac{\mathbf{T\omega}}{\mathbf{IV}} \tag{5}$$

One way to approximate η_{EM} is to calculate the power loss factors and hence the total loss for given design and operational conditions. Lowry and Larminie[18] divide the major sources of loss into four main sections which are generally the same in all motor types and give the total loss relation as shown in Eqn. 6, which can be applied to all motor types. Here, k_c, k_i and k_w are inefficiency constants associated respectively with copper, iron, and windage losses that change with motor torque and speed. The constant, C, designates inefficiency due to all other losses which are independent of torque or speed. These constants can be found based on experimentation or regressions.

$$\mathbf{Total\ Loss = k_c T^2 + k_i \omega + k_w \omega^3 + C} \tag{6}$$

Then, since the efficiency is given by the ratio of output power to the input power (which is the output power combined with total losses), η_{EM} can be calculated by Eqn. 7.

$$\eta_{\mathbf{EM}} = \frac{\mathbf{T\omega}}{\mathbf{T\omega + k_c T^2 + k_i \omega + k_w \omega^3 + C}} \tag{7}$$

Voltage variations from low to high values are usually necessary to control the speed of the motor. The Power Management and Distribution unit (PMAD) is used to regulate the voltage according to the electric motor power requirements. In this study, the PMAD was modeled as a power converter embedded into the electric motor model with its own separate efficiency. When it is desired to control the motor speed, the PMAD converts the system voltage into the motor supply voltage, and hence, the motor speed changes according to the equations given above.

Table 3 shows the electric motor model input and outputs as implemented in Pacelab SysArc. Thanks to the input-output toggle capability of the tool, if motor current and/or voltage are unknown, but torque and/or rotational speed are known, then their input-output position can be swapped. Furthermore, motor weight is calculated from power-to-weight ratio and rated power of the electric motor. The port parameters are designated with a "*" sign in the table.

D. Propeller Speed Reduction Unit (PSRU)

The PSRU is a gearbox which transfers the rotational motion of the motor output shaft to the propeller via speed reduction. Electric motors run at higher efficiency at higher rotational speeds relative to propellers, which are more efficient at lower speeds due to tip speed and structural restrictions. Therefore, unless the electric motor is a direct drive motor, a PSRU is necessary to get the highest efficiency from both the motor and the propeller.

PSRU was modeled using the relationship between the electric motor angular speed (ω_{EM}) and the propeller angular speed (ω_{prop}) through a predefined gearbox ratio (R_g) as given in Eqn. 8. The input and

Table 3. Model input and output parameters of the Electric Motor with embedded PMAD

Inputs			*Outputs*		
Parameter	Units	Description	Parameter	Units	Description
$(P/W)_{EM}$	[kW/kg]	Motor P/W ratio	W_{EM}	[kg]	Motor weight
$P_{rated,EM}$	[kW]	Motor rated power	T	[Nm]	Motor torque
ω_{EM}	[rad/s]	Motor speed*	Iron Loss	[kW]	Iron Losses
P_{mech}	[kW]	Mechanical power*	Copper loss	[kW]	Copper losses
k_i	[Nm]	Iron loss constant	Windage loss	[kW]	Windage losses
k_c	[rad/s (Nm)$^{-1}$]	Copper loss constant	*Total Loss*	[kW]	Total power loss
k_w	[Nm (rad/s)$^{-2}$]	Windage loss constant	η_{EM}	%	Motor efficiency
C	[Nm/s]	Other loss constant	P_{el}	[kW]	Electrical power
k_T	[Nm/A]	Torque constant	$I_{in,EM}$	[A]	Motor current
η_{PMAD}	%	PMAD efficiency	$V_{in,EM}$	[V]	Motor voltage
$(P/W)_{PMAD}$	[kW/kg]	PMAD P/W ratio	$P_{PMAD,in}$	[kW]	Power into PMAD
$P_{rated,PMAD}$	[kW]	PMAD rated power	$I_{in,PMAD}$	[A]	Current going into PMAD
$V_{in,PMAD}$	[V]	PMAD Voltage*	W_{pc}	[kg]	PMAD weight

output parameters for the Pacelab SysArc model are shown Table 4 and the port parameters are designated with a "*" sign. The angular speed of the propeller, ω_{prop} can be calculated through the required power at a given instance and propeller characteristics.

$$\mathbf{R_g} = \frac{\omega_{\mathbf{EM}}}{\omega_{\mathbf{prop}}} \tag{8}$$

Table 4. Model input and output parameters of the PSRU

Inputs			*Outputs*		
Parameter	Units	Description	Parameter	Units	Description
P/W	[kW/kg]	Power to weight ratio	W_{pc}	[kg]	Component weight
P_{nom}	[kW]	Nominal power	ω_{EM}	[rad/s]	Motor speed
R_g		Gear ratio	P_{in}	[kW]	Input power
η_{PSRU}	%	Component efficiency			
P_{out}	[kW]	Output power*			
ω_{prop}	[rad/s]	Propeller speed*			

III. Baseline Aircraft Selection

The first step in the analyses is selecting a baseline aircraft on which the architecture changes will be made. In this work, the baseline aircraft was selected to be the Dornier 328 Turboprop, which is a regional turboprop commuter plane. The authors deemed a regional airliner more suitable as a preliminary step to hybrid-electric analysis compared to larger commercial aircraft. Detailed technical data of this aircraft was provided by 328 Design GmbH.[21] A summary of the aircraft specifications are shown in Table 5.

The baseline aircraft was modeled in Pacelab with matching geometry and performance of the Dornier 328. A 3D drawing of this model is shown in Figure 4.

Table 5. Dornier 328 General Specifications[21]

Seating:	
Crew	3
Passengers	31
Powerplant:	
Engines	Pratt & Whitney Canada - PW 119B
Takeoff Power	2 x 2180 shp
Weights:	
MTOW	13990 kg
Typical OEW (incl. crew)	8900 kg
Max. Fuel	3416 kg
Max. Payload	3671 kg
Performance:	
Power Loading, W_{TO}/P_{SL}	4.30 kg/kW
Wing Loading, W_{TO}/S	349.8 kg/m^2
Takeoff Field Length	1,088 m
Max Cruise Speed (at 95% MTOW)	620 km/h

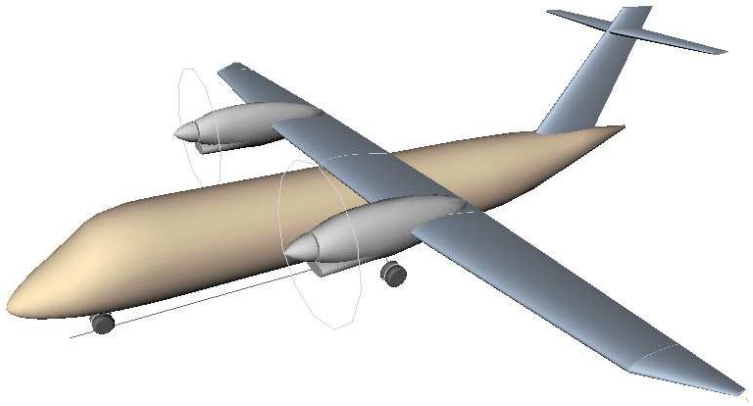

Figure 4. 3D drawing of the baseline aircraft modeled in Pacelab

IV. Design Mission Profile Definition

In order to compare mission level MoPs of the retrofitted designs with the baseline aircraft, a mission profile which is very similar to the design mission of the Dornier 328 was defined in Pacelab. Figure 5 shows the flight profile along with some prominent characteristics of each segment. These characteristics will be kept fixed for competing architectures. The range of the baseline aircraft for the mission payload of 2790 kg is 1140 NM, with a cruise segment of 958 NM. However, the range of retrofitted designs with different architectures will vary due to keeping MTOW fixed, as explained previously. Finally, 5% of the trip fuel was set as the contingency fuel.

V. Hybrid Electric Propulsion Architecture

There are mainly two powertrain configurations for hybrid-electric propulsion: series and parallel; as depicted in Figure 1. A combination of the two is also possible but so far has not been very favorable since hybrid electric vehicle technology is still at the development stage.[22]

In the series configuration the engine is decoupled from the powertrain, and therefore, can run at its peak

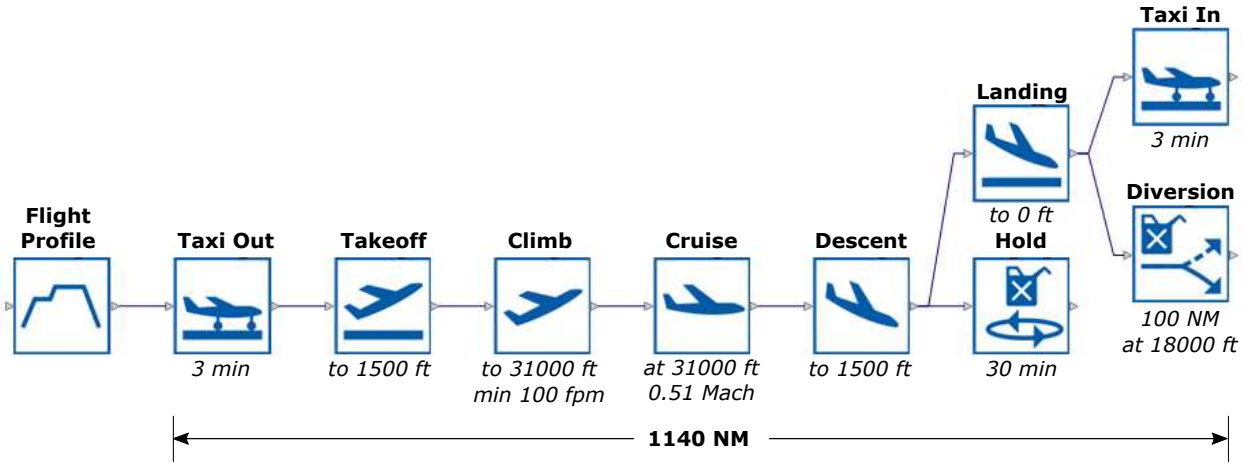

Figure 5. The design mission profile on Pacelab SysArc

efficiency independent from the RPM of the transmission system. This also gives flexibility in terms of its location. However, an extra generator must be employed which brings weight penalty to the system.[23]

The parallel configuration enjoys the weight savings as it only requires an electric motor and a fuel burning engine. The propulsion devices can also be downscaled without any loss in the maximum power. However, there exists a mechanical coupling in this configuration which increases the control complexity.[23]

For the scope of this work, parallel configuration will be utilized. Since this paper does not cover finding optimum hybridization strategies, a single strategy was selected to keep the focus on the effects of PG&D subsystems. Accordingly, hybridization will be effective only during the cruise segment. The rest of the flight segments will be flown solely with the turboprops.

A. Sizing Methodology

The first step of this hybrid sizing methodology is to calculate the power requirements from each engine and motor. To this end, a hybridization factor must be defined. Hybridiztion factor describes the electric power rating as a percentage of the overall maximum power that the vehicle can supply and can be defined as follows:[24]

$$\mathbf{HF} = \frac{P_{EM,max}}{P_{total}} \tag{9}$$

where $P_{EM,max}$ is the maximum power of the electric motor and P_{total} is the sum of the maximum powers of the electric motor and fuel burning engine ($P_{FB,max}$) as shown in Eqn. 10. Here, the fuel burning engine is the turboprop engine of the baseline aircraft. Since $P_{FB,max}$ is known for the baseline aircraft, $P_{EM,max}$ can be obtained from Eqn. 9 for a given hybridization factor. This maximum power corresponds to the rated power of the electric motor and therefore will be the key parameter to size the motor, as shown previously in Table 3.

$$\mathbf{P_{total}} = P_{EM,max} + P_{FB,max} \tag{10}$$

A closer look to the power flow in a parallel hybrid electric configuration is provided by Figure 6. For this configuration, it is assumed that the power requirement of the electric propulsion branch can be decoupled from that of the fuel burning engine branch. Moreover, the percent contribution of each propulsion unit (motor or engine) to the overall power requirement will be dictated by the hybridization factor and kept constant throughout the hybridized flight segment, as given by Eqns. 11 and 12. For instance, if the hybridization factor is set to 10%, then 10% of the total power required is supplied by the electric motor(s) and the remaining 90% will come from the fuel burning engine(s). Since there are two turboprop engines on the baseline aircraft, it means that each engine will supply 45% of the total power required. Similarly, if there are two electric motors, then each will contribute to the 5% of the total power requirement.

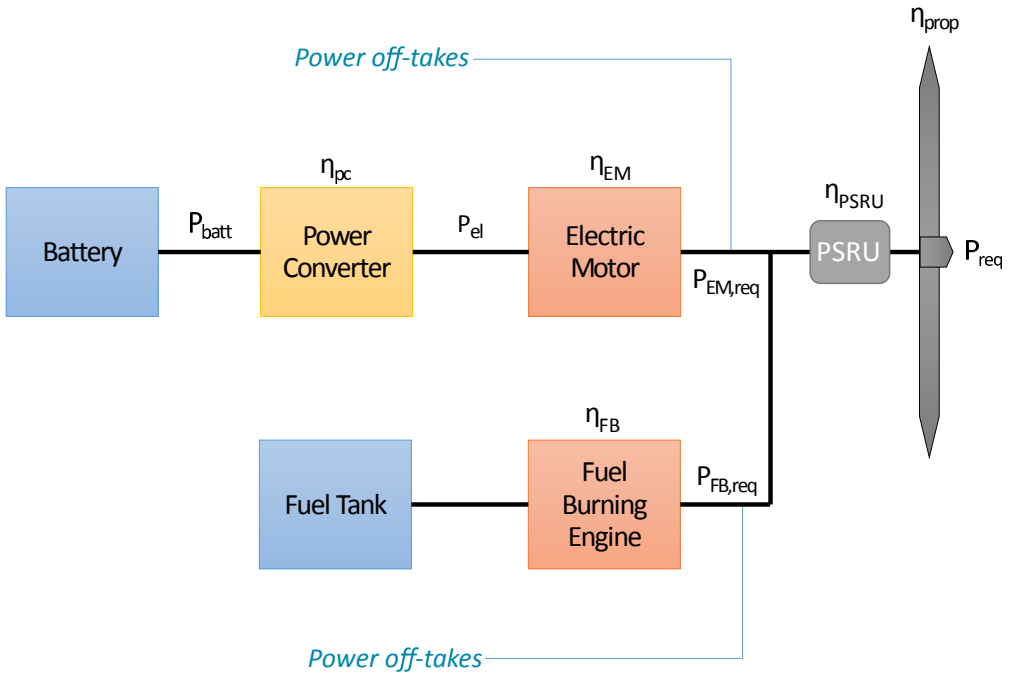

Figure 6. A parallel HEP architecture shown for a single propeller

$$\mathbf{P_{EM,req}} = \mathbf{HF} * \mathbf{P_{req,total}} \tag{11}$$

$$\mathbf{P_{FB,req}} = (\mathbf{1} - \mathbf{HF}) * \mathbf{P_{req,total}} \tag{12}$$

where total power required $P_{req,total}$ is a sum of power off-takes and propulsive power scaled by the inefficiencies in propeller and PSRU, as given in Eqn. 13.

$$\mathbf{P_{req,total}} = \mathbf{P_{off-takes}} + \frac{\mathbf{P_{req}}}{\eta_{\mathbf{prop}} * \eta_{\mathbf{PSRU}}} \tag{13}$$

The required propulsive power to fly the mission anytime during flight is given by Eqn. 14 where D is drag, V is speed, W is instantaneous aircraft weight and h is altitude of the mission leg designated by subscript i. It is assumed that these parameters and hence the power required are constant during each mission leg, i.

$$\mathbf{P_{req,i}} = D_i V_i + \frac{d}{dt}\left(\frac{W V_i^2}{2g} + W h_i\right) \tag{14}$$

The required power from the electric motor ($P_{EM,req}$) is equal to the mechanical (shaft) power of the motor P_{mech} as given in Eqn. 2. The amount of power drawn from the battery is then calculated by scaling $P_{EM,req}$ with electric motor, power converter and battery efficiency factors as described previously. The PG&D subsystems excluding the battery is sized by the maximum power requirement during the cruise segment and their respective power-to-weight ratios. Battery weight is obtained from the total energy requirement during cruise and battery specific energy.

A generalized sizing flowchart is shown in Figure 7. The enumarated steps are summarized as following:

1. Guess an initial battery weight and set SOC to 100%
2. Add battery weight (along with other PG&D subsystem weights) to the baseline aircraft weight (the fuel weight is budgeted such that MTOW is kept constant)
3. Use Eqns. 13 and 14 to calculate overall power requirement to fly mission leg i during time interval dt

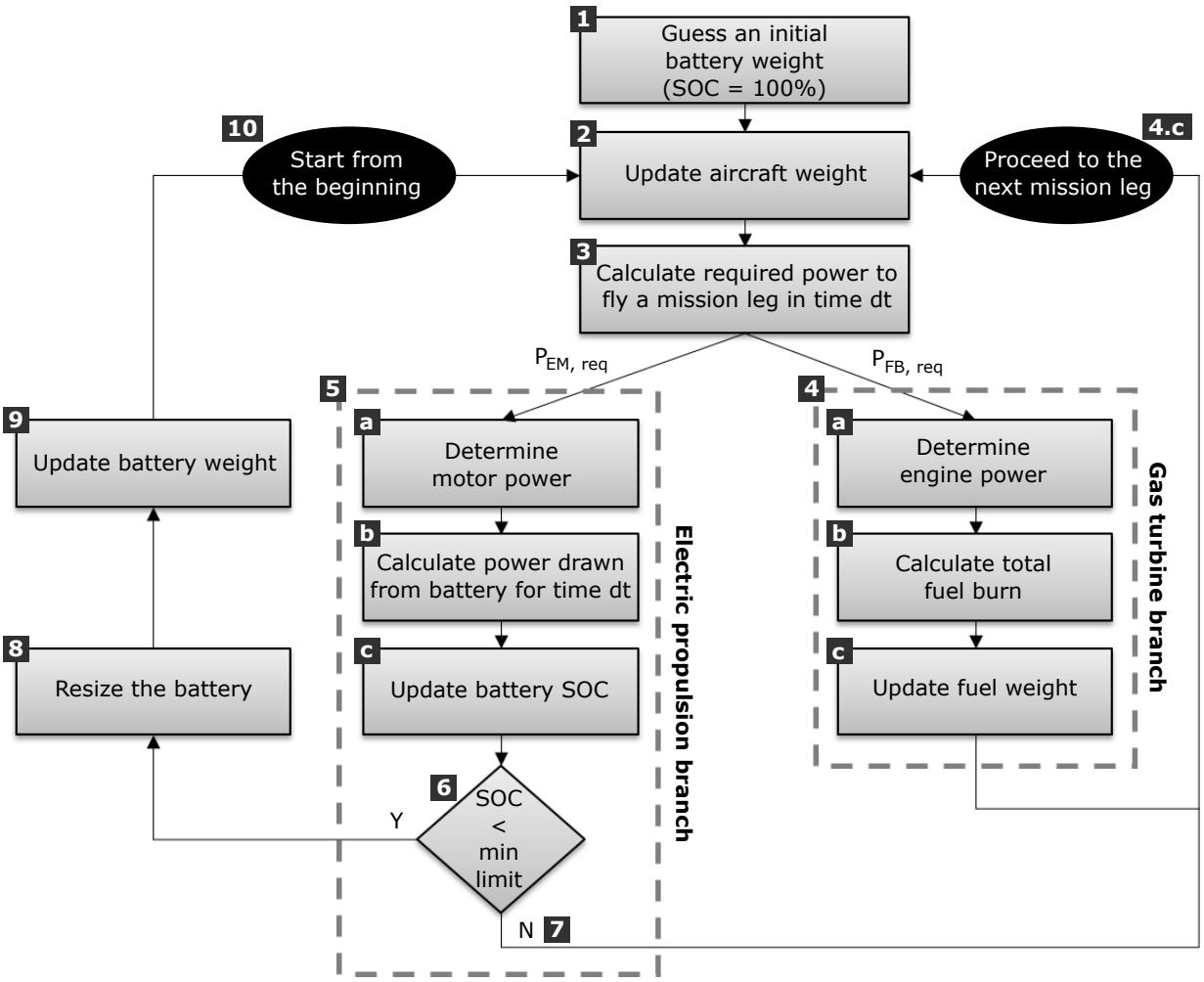

Figure 7. Hybrid electric propulsion sizing flowchart

4. Gas turbine branch:
   (a) Determine required power for the fuel burning engine(s) from Eqn. 12
   (b) Find the amount of fuel burn for the given engine power rating
   (c) Update remaining fuel weight
   (d) Update instantaneous aircraft weight
5. Electric propulsion branch:
   (a) Determine required power for the electric motor(s) from Eqn. 11
   (b) Scale the electric motor power with component inefficiencies up to the battery and calculate the current drawn out of the battery
   (c) Calculate battery voltage and update battery SOC
6. Check whether SOC remains above the minimum SOC limit
7. If SOC is above the minimum limit, carry on with the next mission leg
8. If SOC is below the minimum limit, resize the battery (add more cells to the pack or improve battery technology)

9. Calculate the new battery weight

10. Restart from step 2

B. Building Up the Architecture

The aforementioned PG&D subsystem models were placed into the vehicle and the hybrid electric propulsion architecture was created as demonstrated in Figure 8. In this architecture, there are two electric motors connected to each propeller in parallel and fed by a single battery pack. The nominal voltage of the system was set to 270 V. Two sample secondary subsystems per motor and per engine were also connected via generators. These are arbitrarily placed dummy subsystems with negligible effect on the overall power requirement, but connected to the system to illustrate power off-takes.

After the subsystems were positioned inside the baseline aircraft, the logical connections were then physically connected (i.e. physically wired) by Pacelab SysArc. Electrical wiring is automatically performed by the tool which uses an automatic routing algorithm to find the shortest possible route between two system components along the previously defined pathways. Figure 9 depicts the Dornier 328 with the PG&D subsystems right after the routing algorithm was performed. The electrical cables are shown as green lines traveling between the subsystem components in Figure 9.

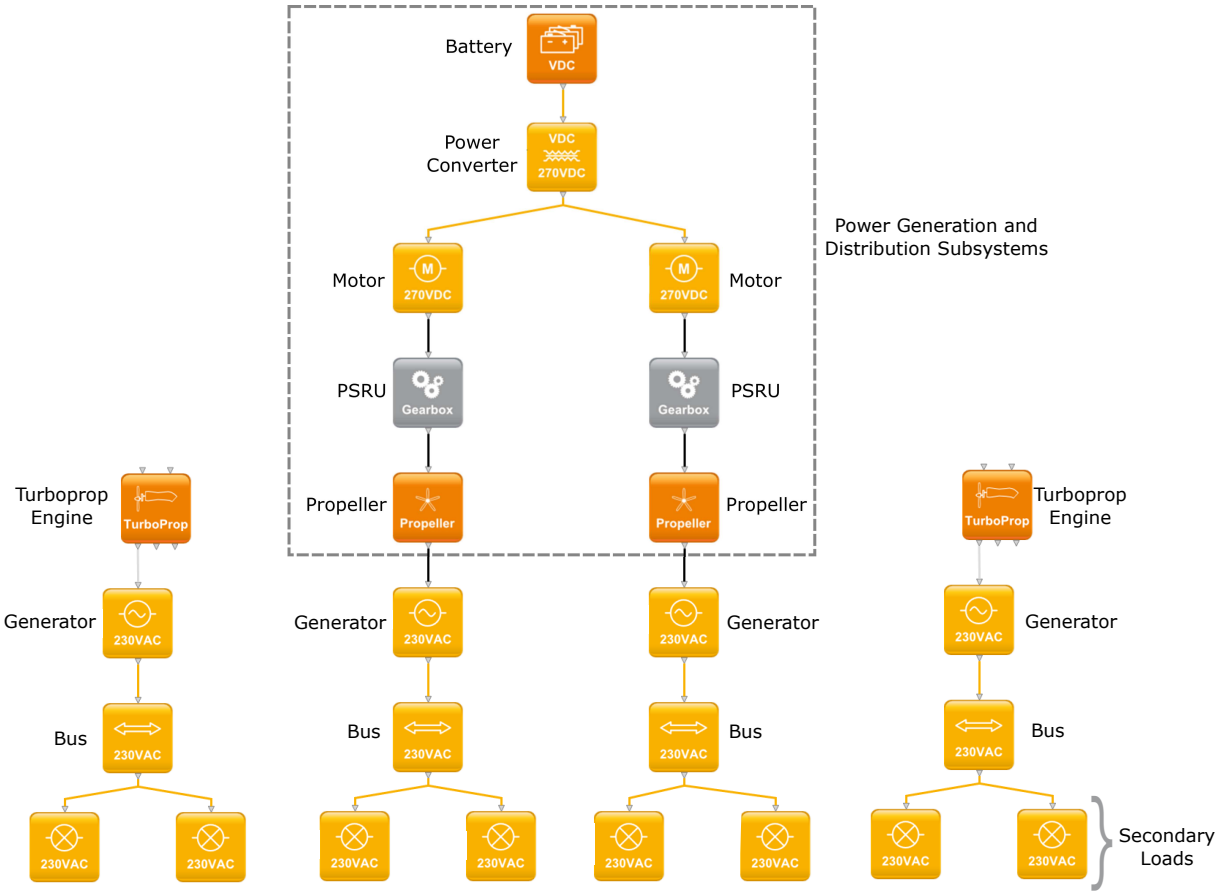

Figure 8. The parallel hybrid electric architecture

VI. Performance Evaluation of Parallel HEP Architectures

In this section, the developed PG&D subsystem models will be compared in terms of different technology levels and hybridization factors under the parallel hybrid electric propulsion architecture explained previously. First, sensitivity to level of hybridization and subsystem performance characteristics will be analyzed at the

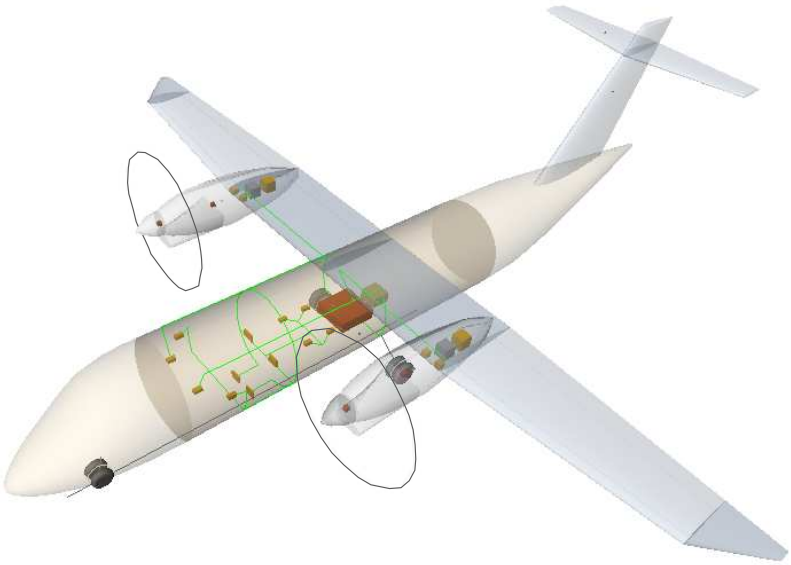

Figure 9. PG&D subsystem components have been placed into the baseline aircraft and physically connected through electrical wiring

subsystem, vehicle and mission levels. Then, competing architectures will be chosen and compared in terms of the previously determined MoPs.

A. Sensitivity Analysis at Subsystem, Vehicle and Mission Levels

In order to investigate the effects of changing subsystem characteristics both at vehicle and mission levels, a design variable space was created for subsystem performance characteristics as shown in Table 6.

Table 6. The design variable space for sensitivity analysis

Design Variable	Minimum	Maximum	Units
Hybridization Factor	0	50	%
Battery Specific Energy	200	5000	Wh/kg
Electric Motor P/W	2.2	16	kW/kg
Power Converter P/W	2.2	19	kW/kg

The minimum limits of the battery specific energy, motor specific power and converter specific power reflect the current state-of-the-art technology levels for these components.[9] As a matter of fact, recent advances in electric motors enabled higher power-to-weight ratios, such as Siemens' electric motor for aircraft which has a state-of-the-art power-to-weight ratio of 5 kW/kg.[25] However, most of the other electric motors still can not deliver as much power at a similar specific power, and hence the minimum limit was set to be 2.2 kW/kg to be more representative.

The maximum specific power limits for the motor and power converter were chosen based on NASA 15-year goals.[9,26] Since PMAD was also modeled as a power converter, its technology level was set equal to that of power converter. Since it was expected that the battery would turn out to be the heaviest component among the PG&D subsystems, the maximum limit of battery specific energy was set to a rather aggressive value in order to study its effect on range.

The minimum level of hybridization of 0% in this context means that although PG&D subsystems were placed inside the baseline aircraft, the propulsive power is solely supplied by the turboprops. Therefore, when the hybridization factor is 0%, the PG&D subsystems are sized based on the power required by the secondary subsystems. Due to the nature of mission performance calculations in Pacelab SysArc, the maximum value of the hybridization factor was limited to 50% rather than 100% (fully electric cruise).

The sizing of the subsystem components except for the battery are done based on user-specified power-to-weight ratios and rated powers, as discussed previously. However, in order to automate the sizing process for sensitivity analysis, an additional iteration was performed such that the rated power of these subsystems were chosen automatically to be 5% greater than the maximum power required from the subsystems during cruise. The determination of the maximum required power from each subsystem and the weight of the overall system are interdependent, and hence an iteration is necessary.

In order to alleviate the computational burden of simulating the response to every combination of design metrics, surrogate modeling approach was used. To this end, a space-filling design of experiments (DoE) was generated within the design variable space shown in Table 6. This DoE was fed into Pacelab SysArc and the response data of various response metrics were collected. Then, a prediction formula for each response metric was obtained using the Gaussian process. These prediction formulas were tested for goodness of the fit and validated with data which was not used to create the formulas. Then, prediction profilers were created to study the sensitivity of the vehicle and mission level MoPs to changing subsystem characteristics and level of hybridization. The results are given in the prediction profiler in Figure 10.

In Figure 10, the prediction profiler with prediction traces for each variable gives the predicted response as one design variable is changed while the others are kept constant at their current values and therefore makes it possible to see the effect of each variable separately. The values shown in red on the horizontal axis are the median values within the limits of each design variable; and similarly, the values shown in red on the vertical axis are corresponding predicted responses.

It can be seen in Figure 10 that total PG&D subsystem weight (sum of all electric motors, converters, gearboxes, and battery) increases with increasing level of hybridization, because higher and higher power is drawn from PG&D subsystems. The overall weight changes end up increasing the OEW. Since MTOW is kept fixed, less fuel can be taken on board. Hence, both the trip fuel weight and total fuel weight drop. As a result, cruise stage length and mission range decrease significantly, and therefore less propulsive energy is required during cruise.

An obvious result is seen on the battery specific energy column. Aircraft range increases as battery technology advances in terms of specific energy, as expected. Since the battery weighs less for increasing specific energy and the equipment weight factors are kept fixed, OEW also drops in a similar trend as total PG&D weight. The extended range is not only due to having greater battery capacity, but also carrying more fuel on board thanks to the lighter battery pack.

Advances in motor and converter technology in terms of higher power-to-weight ratios benefits longer range by reducing total PG&D subsystems weight and OEW. In the chosen architecture shown in Figure 8, there are three converters (two of which are PMAD) and two motors. Only less than half of the power drawn from the converter connected to the battery is drawn individually from the PMAD units and electric motors as a result of the chosen architecture. Since the rated power of these components are determined by the maximum required power, power converter weight exceeds motor and PMAD weights. That's why the effect of the converter power-to-weight ratio is greater than that of the electric motor. The effect of the converter power-to-weight ratio on the response metrics fades out after a certain value (about 9 kW/kg for the conditions given in red in Figure 10) as the weight of the converter and PMAD units become negligible. A similar phenomenon is true for the electric motor power-to-weight ratio, where the effect on the response metrics diminish after about 8 kW/kg for the conditions given in red in Figure 10.

Figure 10 demonstrates the sensitivities to the design metrics at mission level in terms of required energy, range and fuel weight; aircraft level in terms of OEW; and subsystem level in terms of total PG&D subsystems weight. A closer look at the subsystem level is provided in Figure 11. In this figure, the sensitivities of the individual subsystem components to the same design metrics can be inspected.

When the PG&D subsystems are compared individually, the heaviest component is the battery regardless of the hybridization factor and subsystem technology levels. The effect of battery specific energy on motor, converter and PMAD weights are negligible. On the other hand, changing motor and converter power-to-weight ratios seem to affect battery weight. The main reason behind the battery weight reduction at lower motor and converter power-to-weight ratios is that because motor, converter and PMAD become heavier while MTOW is kept fixed, the range of the aircraft reduces, as previously shown in Figure 10. Thus, to balance the required energy provided by the battery, the battery is sized to be smaller.

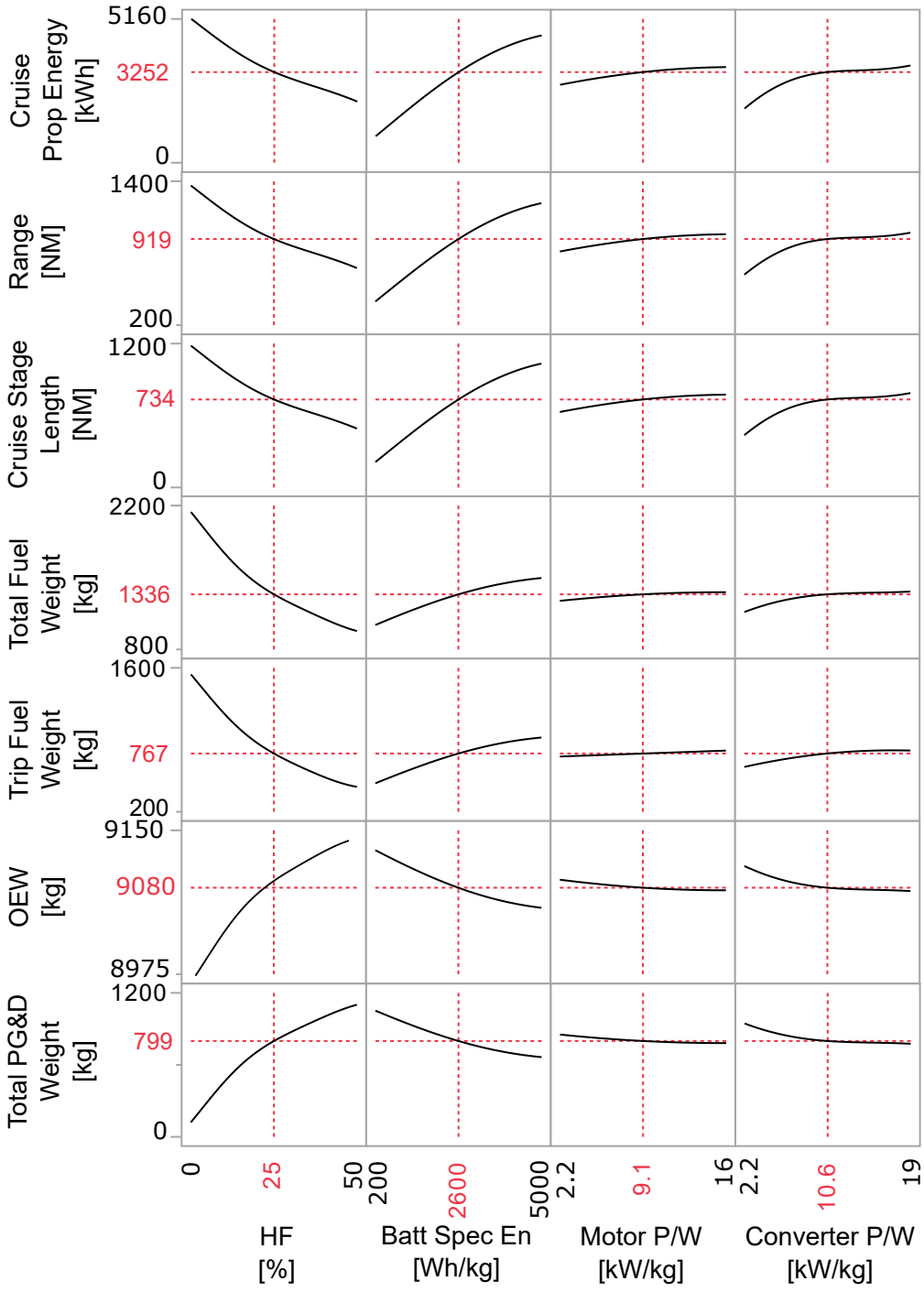

Figure 10. The prediction profiler showing predicted response at system and mission levels for changing design variables ("HF" stands for "hybridization factor")

The hybridization factor and required rated powers of converter, motor and PMAD are *almost* directly proportional. This means that although the technology levels of the battery, motor and converter change the weight of the total PG&D weight, this weight change is negligible compared to overall weight of the aircraft; and therefore, does not impact the maximum power required from the power converter, motor and PMAD.

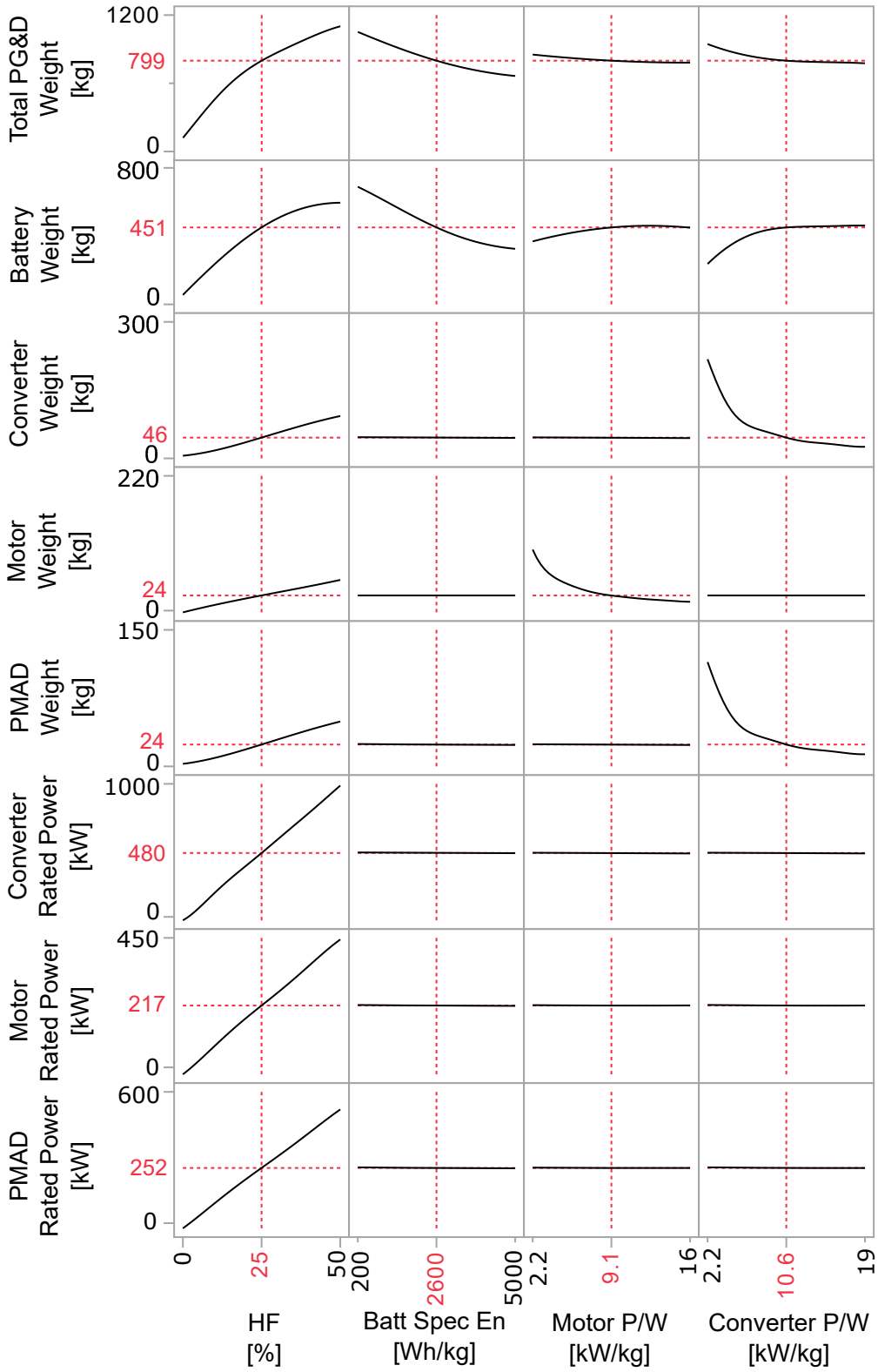

Figure 11. The prediction profiler showing predicted response at the subsystem level for changing design variables

B. Architecture Comparison

In this study, we compared three different technology levels in candidate parallel hybrid electric propulsion architectures. These are according to the technology levels of: 1. current state of the art (SOA), 2. NASA 15-year goals and 3. a break-even point for the Dornier 328. These three sets were divided into two groups with group (a) evaluated at 25% level of hybridization and with group (b) evaluated at 50% level of hybridization. The properties of these candidate architectures are given in Table 7.

Table 7. Characterization of the candidate architectures

	Units	Arch. 1-a	Arch. 1-b	Arch. 2-a	Arch. 2-b	Arch. 3-a	Arch. 3-b
HF	%	25	50	25	50	25	50
Batt Spec Energy	Wh/kg	250	250	600	600	5000	5000
Motor P/W	kW/kg	5	5	16	16	16	16
Converter P/W	kW/kg	2.2	2.2	19	19	19	19

The third architecture differs from the second one only in terms of a much higher battery specific energy. This value of battery specific energy was chosen in order to be able to reach a break-even point, i.e. an architecture setting that would produce the same aircraft range as the baseline aircraft. The results (along with the percent change over the baseline aircraft vehicle and mission level metrics) are listed in Table 8.

Table 8. Comparison of the candidate architectures in terms of subsystem, vehicle and mission level performance metrics ("r-Power" stands for "Rated Power")

	Units	Arch. 1-a	Arch. 1-b	Arch. 2-a	Arch. 2-b	Arch. 3-a	Arch. 3-b
Cruise Prop Energy	kWh	758.24	N/A	1628.39	820.66	4959.67	4086.65
% change		-81.80%	N/A	-60.90%	-80.30%	+19.08%	-1.88%
Range	NM	351.69	N/A	549.25	368.85	**1304.15**	**1102.80**
% change		-69.15%	N/A	-51.82%	-67.65%	**+14.40%**	**-3.26%**
Cruise Stage Length	NM	166.29	N/A	364.32	183.31	1120.55	917.59
% change		-82.66%	N/A	-62.00%	-80.88%	+16.87%	-4.30%
Total Fuel Weight	kg	943.53	N/A	1106.84	944.53	1504.89	1054.45
% change		-58.63%	N/A	-51.48%	-58.59%	-34.02%	-53.77%
Trip Fuel Weight	kg	402.71	N/A	559.57	402.34	944.63	507.17
% change		-76.21%	N/A	-66.95%	-76.24%	-44.21%	-70.04%
OEW	kg	10265.60	N/A	10106.72	10266.24	9655.80	10205.97
% change		+14.89%	N/A	+13.11%	+14.90%	+8.07%	+14.23%
Total PG&D Weight	kg	1131.39	1129.78	993.16	1130.78	656.04	1037.69
Battery Weight	kg	187.39	27.31	634.64	693.16	373.27	625.26
Converter Weight	kg	221.63	342.74	25.47	51.96	24.91	51.73
Motor Weight	kg	40.89	99.25	13.17	30.37	13.17	30.37
PMAD Weight	kg	116.33	181.32	13.34	27.30	13.12	27.19
Converter r-Power	kW	491.45	947.87	489.11	983.06	481.85	973.21
Motor r-Power	kW	233.05	442.00	219.20	439.35	217.54	439.50
PMAD r-Power	kW	257.82	514.53	253.40	514.01	249.74	512.74

The first set of architecture with current SOA PG&D subsystems weighs too heavy to reach the baseline range. Architecture 1-b is so heavy that the aircraft with this architecture cannot even fly the cruise segment, and therefore the results are not applicable for this case. It can also be seen from Table 8 that Architectures 2-a and 2-b also misses the baseline aircraft range by a lot. This means that even if the NASA 15-year goals are reached, such a retrofit would not give the same performance as the conventional fuel burned baseline

aircraft. In fact, in order to reach the baseline aircraft range of 1140 NM with 50% level of hybridization, battery specific energy must be about 5000 Wh/kg, while the other subsystems are kept at corresponding NASA 15-year goal values.

Comparing all six competing architectures, Architectures 3-b results in a range very close to the baseline, and therefore it can be seen as the break-even point for 50% hybridization. Moreover, a longer range can be achieved with the same subsystem characteristics when the hybridization factor is 25%. Although Architecture 3-a can fly for a higher range, it only saves about 44% trip fuel; whereas Architecture 3-b not only can cover about the same distance as the baseline aircraft, but also brings 70% trip fuel savings.

This study shows that only very aggressive technology infusions would allow replacing half of the fuel energy by electric energy required for the cruise segment in order to reach similar range goals as the Dornier 328 aircraft. However, aircraft are usually sized for much greater range requirements on paper than they actually fly in real operations. For instance, a typical flight for the Dornier 328 usually lasts less than 1 hour covering a range of about 400 NM. Therefore, relaxing the range requirement along with technology infusion enables feasible architectures, such as Architectures 2-a, 3-a and 3-b. Architectures 1-a and 2-b miss the 400 NM range requirement by 12% and 7.8%, respectively. Since the range of all analyzed architectures is limited by weight and not by tank capacity, and the battery weight is the predominant fraction of the total PG&D weight, the possibility of a quick removal of the batteries and temporarily substituting battery weight with extra fuel would give operators the flexibility to increase the range on certain routes while benefiting from the fuel efficiency of the PG&D subsystems on the majority of the routes.

VII. Conclusion and Future Work

This paper presented a method to integrate physics-based PG&D subsystem models within a hybrid parallel architecture. The main objective was to evaluate the impact of changing subsystem performance characteristics at system and mission levels. To this end, a retrofit study was performed on the Dornier 328 by employing a parallel hybrid electric architecture while keeping its MTOW constant.

Hybridization only took place during the cruise segment, and rest of the segments were flown solely on the two turboprop engines of the baseline aircraft. The turboprop engines were kept as-is, whereas the electric motors were sized for different hybridization factors. The battery was sized according to the electric energy requirement that varied with the hybridization level using the sizing methodology given in Figure 7. Iterations took place as the PG&D subsystems were sized until the weights of the PG&D subsystems, changing structures and fuel converged such that MTOW matched to that of the baseline aircraft.

The developed subsystem models and the sizing methodology were then used in sensitivity analysis and architecture comparison. Sensitivity analysis were conducted to reveal the effects of varying the subsystem performance characteristics and level of hybridization on subsystem weight and power capability, OEW, fuel weight, overall energy required to fly the cruise segment and range. A design space stretching from today's technology to NASA's 15-year goals was created to study the ever-changing technology at the subsystem level.

As a result of the sensitivity analysis, it was seen that the greatest impacts on range was done by the hybridization factor and battery specific energy. Shifting to 50% electric cruise while keeping the battery specific energy constant at a relatively low value in the design space resulted in significant range cuts for the retrofitted aircraft compared to the baseline aircraft. An opposite effect was seen when the battery specific energy was increased up to 5 kWh/kg, as expected. However, technology advances in electric motor and power converter in terms of power-to-weight ratios did not create as big of an impact as the battery. Their impact was almost negligible especially at high power-to-weight ratios, mostly because their weights become very small compared to that of the battery. It's worth noting that if the hybridization also took place during more power-demanding segments of the flight, such as takeoff, then the electric motors and the power converter would have been sized according to higher power needs than the maximum power required during cruise. In that case, their technology levels might have made a greater impact on the mission level. Finally, the sensitivity analysis at the subsystem level revealed the interdependencies between the PG&D subsystems during the sizing process.

An architecture comparison was made between three sets of different architectures. These three sets represented the subsystem characteristics for current state of the art, NASA 15-year goals and NASA 15-year goals with a much advanced battery with 5 kWh/kg specific energy. Each set was split up to two different levels of hybridization, namely, 25% and 50%; making it a total of six competing architectures.

These candidates were then compared by evaluating their performance at the subsystem, vehicle and mission levels. It was seen that electrifying 50% of the cruise with today's state of the art subsystems is not possible for the Dornier 328, as the total PG&D weight and resultant OEW exceeds the allowable limits. On the other hand, 25% hybridization is possible in the expense of losing about 70% of the design mission range. The second set of architectures which represented the NASA 15-year goals also did not manage to reach to the baseline aircraft's range. However, since a typical mission for the Dornier 328 is about 400 NM (much less than the design mission range requirement of 1140 NM), they can still be utilized provided that each subsystem reaches the projected technology level. Finally, the final set of architecture which included a much improved battery performed much better than the other two competing sets by reaching to the mission design range goal. The 25% hybrid and 50% hybrid versions of this set also enjoyed fuel savings of about 34% and 54%, respectively, compared to the baseline aircraft.

Although the subsystem analyses were made at a rather detailed level, there is still more to add to the subsystem models. These models do not assume thermodynamic losses, and cooling was not included in the scope of this study. Furthermore, although the models and the sizing procedure were developed to include cable weights and losses, this study neglected such considerations to remove any uncertainties that would be caused by carrying very large amount of currents. A future study is underway to include these phenomena as well as volumetric considerations.

Furhermore, the retrofit study presented here will be expanded to a sizing study where the baseline aircraft will be resized to meet the original payload-range working capacity and low-speed performance in the future. The hybridization will also be extended to the whole design mission and battery discharging-recharging strategies will be analyzed.

References

[1]ICAO, "Environmental Report 2013: Aviation and Climate Change," .

[2]European Commission Climate Action, "Reducing Emissions From Aviation," [online article], 2015, URL: http://ec.europa.eu/clima/policies/transport/aviation/index_en.htm [cited on 28 Nov. 2015].

[3]ICAO, "Resolution A37-19: Consolidated statement of continuing ICAO policies and practices related to environmental protection Climate change," Tech. rep., Montreal, October 2010.

[4]ICAO, "New ICAO Aircraft CO2 Standard One Step Closer To Final Adoption," Press Release, February 2016.

[5]IATA, "IATA Technology Roadmap," June 2013.

[6]Hornung, M., Isikveren, A. T., Cole, M., and Sizmann, A., "Ce-Liner Case Study for eMobility in Air Transportation," AIAA, Los Angeles, CA, August 12-14 2013.

[7]Bradley, M. K. and Droney, C. K., "Subsonic Ultra Green Aircraft Research: Phase II Volume II Hybrid Electric Design Exploration," Tech. rep., Boeing Research and Technology, Huntington Beach, California, April 2015.

[8]Madavan, N. K., Del Rosario, R., and Jankovsky, A. L., "Hybrid-Electric and Distributed Propulsion Technologies for Large Commercial Transports: A NASA Perspective," Special Session on Future Electric Aircraft - Systems, IEEE, Montreal, Canada, 20-24 Sep. 2015.

[9]National Academies of Sciences, Engineering, and Medicine, *Commercial Aircraft Propulsion and Energy Systems Research: Reducing Global Carbon Emissions*, The National Academies Press, Washington DC, 2016.

[10]Isikveren, A. T., Pornet, C., Vratny, P. C., and Schmidt, M., "Optimization of Commercial Aircraft Using Battery-Based Voltaic-Joule/Brayton Propulsion," *Journal of Aircraft*, July 2016, pp. 1–16.

[11]Roskam, J., *Airplane Design Part V - Component Weight Estimation*, Design Analysis and Research Corporation, Kansas, 1999.

[12]Raymer, D. P., *Aircraft Design: A Conceptual Approach*, AIAA Education Series, AIAA, Virginia, 5th ed., 2012.

[13]Mattingly, J. D., Heiser, W. H., and Pratt, D. T., *Aircraft Engine Design*, AIAA Education Series, AIAA, 2nd ed., 2002.

[14]Coffin, J. G., "A Study of Airplane Ranges and Useful loads," Tech. rep., NACA, Tustin, CA, January 1920.

[15]Cinar, G., Emeneth, M., and Mavris, D. N., "A Methodology for Sizing and Analysis of Electric Propulsion Subsystems for Unmanned Aerial Vehicles," 54th AIAA Aerospace Sciences Meeting, AIAA, San Diego, CA, January 4-8 2016.

[16]Cinar, G., Mavris, D. N., Emeneth, M., Schneegans, A., and Fefermann, Y., "Development of Parametric Power Generation and Distribution Subsystem Models at the Conceptual Aircraft Design Stage," 55th AIAA Aerospace Sciences Meeting, AIAA, Grapevine, TX, January 9-13 2017.

[17]Chakraborty, I. and Mavris, D. N., "Heuristic Definition, Evaluation, and Impact Decomposition of Aircraft Subsystem Architecture," 16th AIAA Aviation Technology, Integration, and Operations Conference, AIAA., AIAA, Washington, D.C., 13-17 June 2016.

[18]Lowry, J. and Larminie, J., *Electric Vehicle Technology Explained*, John Wiley & Sons, 2nd ed., June 2012.

[19]Tremblay, O. and Dessaint, L. A., "Experimental validation of a battery dynamic model for EV applications," *World Electric Vehicle Journal*, Vol. 3, No. 1, May 2009, pp. 1–10.

[20]McDonald, R. A., "Electric Propulsion Modeling for Conceptual Aircraft Design," 52nd Aerospace Science Meeting, AIAA SciTech, National Harbor, Maryland, Jan. 2014.

[21]328 Design GmbH, "Dornier 328-100 TP," Company website, August 2013, URL: http://328.eu/wp-content/uploads/2013/06/328-100-turboprop.pdf [cited 22 Nov 2016].

[22]Friedrich, C. and Robertson, P. A., "Design of a Hybrid-Electric Propulsion System for Light Aircraft," 14th AIAA Aviation Technology, Integration, and Operations Conference, AIAA, Atlanta, GA, 16-20 June 2014.

[23]Chau, K. T. and Wong, Y. S., "Overview of Power Management in Hybrid Electric Vehicles," *Energy Conversion and Management*, Vol. 43, No. 15, October 2002, pp. 1953–1968.

[24]Buecherl, D., Bolvashenkov, I., and Herzog, H. G., "Verification of the Optimum Hybridization Factor as Design Parameter of Hybrid Electric Vehicles," Proceedings of the 2009 Vehicle Power and Propulsion Conference, IEEE, Piscataway, NJ, 2009, pp. 847–851.

[25]Siemens AG, "World-record Electric Motor For Aircraft," [company website], Mar. 2015, URL: http://www.siemens.com/press/en/feature/2015/corporate/2015-03-electromotor.php?content[]=Corp [cited on 13 Sep. 2015].

[26]Slingerland, R. and Zandstra, S., "Green Freighter Systems," 46th AIAA Aerospace Sciences Meeting and Exhibit, Reno, Nevada, Jan. 2008.